JOURNAL OF GEOPHYSICAL RESEARCH, VOL. 114, A08302, doi:10.1029/2009JA014195, 2009

Spread F, GPS phase fluctuations, and plasma bubbles near the crest of equatorial ionization anomaly during solar maximum

C. C. Lee,[1] F. D. Chu,[2] W. S. Chen,[3] J. Y. Liu,[3,4] S.-Y. Su,[3,4] Y. A. Liou,[3,4] and S. B. Yu[5]

Received 26 February 2009; revised 26 May 2009; accepted 2 June 2009; published 5 August 2009.

[1] This work is the first attempt to concurrently study the occurrence probabilities of spread F, GPS phase fluctuations, and plasma bubbles near the crest of equatorial ionization anomaly (EIA). The data were observed by an ionosonde, a GPS receiver, and ROCSAT-1 during 2000, the solar maximum year. Results show that the occurrences of the range spread F (RSF) differ from those of the frequency spread F (FSF). For the seasonal variation, the RSF occurrence has the maximum values in March and September, while the FSF occurrence peaks at June. For the nighttime variation, RSF and FSF peak at 2300 and 0300 LT, respectively. Regarding the GPS phase fluctuations, an index Fp is applied to characterize the irregularity strength. The similarity between the $50 < Fp \leq 200$ and RSF occurrences demonstrates that the characteristics of F region irregularities forming $50 < Fp \leq 200$ are mainly related to RSF. The occurrence of $200 < Fp$ is almost absent. The rare event is also found in the observation of plasma bubbles by ROCSAT-1. Furthermore, the seasonal variations in GPS phase fluctuations at the EIA crest and the dip equator have similar trends. This indicates that the F region irregularities of RSF and $50 < Fp \leq 200$ at the EIA crest are originated from the equatorial ionosphere. On the other hand, the seasonal variation in occurrence probability of FSF at the EIA crest is close to that of spread F at midlatitudes. This suggests that the generation mechanisms of FSF and midlatitude spread F might be same, but the further study is required.

Citation: Lee, C. C., F. D. Chu, W. S. Chen, J. Y. Liu, S.-Y. Su, Y. A. Liou, and S. B. Yu (2009), Spread F, GPS phase fluctuations, and plasma bubbles near the crest of equatorial ionization anomaly during solar maximum, *J. Geophys. Res.*, *114*, A08302, doi:10.1029/2009JA014195.

1. Introduction

[2] The equatorial ionization anomaly (EIA) is formed at the geomagnetic latitudes of approximately ±15°, because the plasma in the equatorial F region would be lifted to higher altitudes by the upward $\mathbf{E} \times \mathbf{B}$ drift velocity, and in turn diffuses along the geomagnetic field lines to higher altitudes [*Appleton*, 1946; *Moffett and Hanson*, 1965; *Bramley and Peart*, 1965; *Anderson*, 1973a, 1973b]. Since the plasma density peaks at the crest of EIA in the equatorial and low latitudes, the studies of F region features near this location have been an interest for scientists. Among the features, many scientists have focused on the behaviors of F region irregularities, because the ionospheric irregularities would disrupt the communication of transionospheric signals. For more than 3 decades, numerous works have studied the occurrence of F region irregularities in the EIA crest region in different longitudinal sectors, using ionosonde, VHF/UHF/L band scintillations, as well as fluctuations and depletions of total electron content (TEC) [e.g., *Kulkarni and Rastogi*, 1969; *C.-M. Huang*, 1970; *Y. N. Huang*, 1985; *Mullen et al.*, 1985; *Basu et al.*, 1999; *Chakraborty et al.*, 1999; *Chandra et al.*, 2003].

[3] In the Indian sector, *DasGupta et al.* [1981] and *Chakraborty et al.* [1999] received the 136 MHz signal to investigate the nighttime occurrences of VHF scintillation at Calcutta (23.0°N, 88.5°E; geomagnetic latitude is 12.7°N). *Chandra et al.* [2003] analyzed the spread F recorded by the Ahmedabad ionosonde (23.0°N, 72.4°E; geomagnetic latitude is 14.0°N), and found that the occurrences of both the VHF scintillation and the range spread F (RSF) are maximum at equinoxes, moderate in winter, and minimum in summer during high sunspot years. For the frequency spread F (FSF), they found that it appears frequently in summer. In the western Pacific sector, *C.-M. Huang* [1970] concurrently analyzed the data of scintillation at Taipei (25.0°N, 121.5°E; geomagnetic latitude is 14.5°N) and spread F at Chungli (24.9°N, 121.2°E; geomagnetic latitude is 14.4°N) to study the F region irregularities. He presented that, during high solar activity, both the scintillation and RSF occur most frequently at equinoxes, and the FSF occurrence has a maximum in summer and a minimum in winter. These results are similar to those found by *Y. N. Huang et al.* [1987], which examined the ionosonde data

[1]General Education Center, Ching Yun University, Jhongli, Taiwan.
[2]National Standard Time and Frequency Laboratory, Telecommunication Laboratories, Chunghwa Telecom Company, Ltd., Jhongli, Taiwan.
[3]Graduate Institute of Space Science, National Central University, Jhongli, Taiwan.
[4]Center for Space and Remote Sensing Research, National Central University, Jhongli, Taiwan.
[5]Institute of Earth Sciences, Academia Sinica, Taipei, Taiwan.

0148-0227/09/2009JA014195$09.00

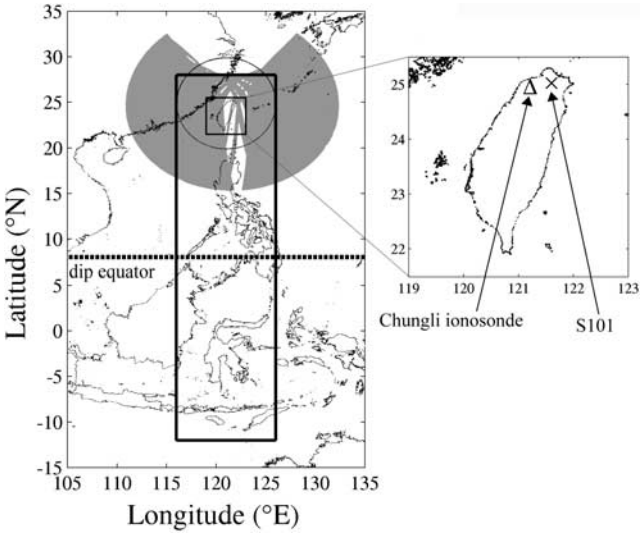

Figure 1. The triangle and cross symbols represent the locations of Chungli ionosonde and S101 GPS stations, respectively. The gray lines are the subionospheric points of the paths for all GPS satellites at the height of 350 km during 2000. The center of circle with a radius of 5° is located at Chungli. The rectangular area marked by solid lines is inside 0 ± 20° geomagnetic latitudes and 121 ± 5° geographic longitudes.

during 1960–1982. Moreover, *Y. N. Huang* [1985] reported that the TEC depletion associated with scintillation are related to RSF. In the Brazilian and African sectors, the RSF occurrence at Cachoeira Paulista (22.5°S, 45°W; geomagnetic latitude is 12.8°S) peaks at December to the solstice (summer) during high sunspot years [*Chandra et al.*, 2003]. This kind of seasonal occurrence was also observed by the L band (1.5 GHz) scintillation at Ascension Island (7.9°S, 14.4°W; geomagnetic latitude is 16°S) [*Mullen et al.*, 1985].

[4] As mentioned above, the *F* region irregularities near the EIA crest in different longitudes have been investigated by many workers. However, the study concurrently using ionosonde, Global Positioning System (GPS), and satellite is not done yet. This study is the first attempt to employ simultaneously the Chungli ionosonde, S101 GPS receiver (25°N, 121.6°E; geomagnetic latitude is 14.5°N), and ROCSAT-1 (now renamed as FORMOSAT-1) to investigate the occurrences of *F* region irregularities near the EIA crest. The data of spread F, GPS phase fluctuations, and plasma bubbles during 2000, the solar maximum year of the 23rd solar cycle, are used in this study. Further, the seasonal and nighttime variations in occurrence probabilities of these three data will be derived to explore the behaviors of *F* region irregularities at the EIA crest in detail.

2. Observations

[5] In this study, we analyze the irregularities data of Chungli ionosonde, S101 GPS receiver and ROCSAT-1 near the EIA crest during 2000. The locations of the ionosonde and GPS receiver are displayed in Figure 1. It is noted that the monthly smoothed sunspot number of the 23rd solar cycle peaked in April 2000 with a value of 120.8.

[6] When the irregularities appear in the *F* region above Chungli, the diffuse echoes, called spread F, would be recorded on ionogram by the Chungli ionosonde. The observed spread F echoes are classified into two types: RSF and FSF, according to the diffusion characteristics [e.g., *Davies*, 1990]. The type of spread F is scaled by manual works from the observed ionogram with a 15-min interval.

[7] For GPS, the irregularities would cause the GPS phase fluctuations in the received signals of the S101 GPS station [*Mendillo et al.*, 2000; *Chen et al.*, 2006; *Chu et al.*, 2008, 2009]. The index, *Fp*, of the GPS phase fluctuations proposed by *Mendillo et al.* [2000] is used to describe the *F* region irregularities. This *Fp* value with a 1-h interval is derived from the temporal variation of TEC for the elevation angle greater than 15° (see *Mendillo et al.* [2000] for detail). The subionospheric points of the paths for all GPS satellites at the height of 350 km are displayed in Figure 1. On the basis of *Mendillo et al.* [2000], two levels of *Fp* values represent the strengths of irregularities: $200 < Fp$ represents very strong irregularities and $50 < Fp \leq 200$ represents that moderate irregularities exist.

[8] Regarding the satellite data, the Ion Trap sensor onboard ROCSAT-1, at 600 km circular orbit with a 35° inclined orbital plane, can measure the ion density at this altitude. When the density depletions appear in the ion density data, the depletions are identified as the plasma bubbles existing in the topside ionosphere (600 km) [*Su et al.*, 2006]. In this study, the plasma bubbles occurring above the Chungli ionosonde (in the circle as shown in Figure 1) are included in the following analysis. It is noted that the center of the circle with a radius of 5°, is located at Chungli.

3. Results

3.1. Occurrence Probabilities of Spread F, GPS Phase Fluctuations, and Plasma Bubbles

[9] Figure 2 shows the seasonal variations in occurrence probabilities of RSF (open square line) and FSF (solid square line) during 2000, observed by the Chungli ionosonde. This seasonal variation in occurrence probability is the percentage of days on which at least one spread F event is observed daily in a month. In Figure 2a (premidnight, 1800–0000 LT), the RSF occurrence has two peaks in March (48%) and September (40%); while the FSF occurrence peaks in June (17%). For the postmidnight (Figure 2b), the RSF occurrences in March, April, and June–September have greater values (30–42%); while the FSF occurrence still has a peak in June (57%). During whole night (Figure 2c), the RSF occurrences are maximum in the equinoctial months, moderate in the summer months, and minimum in the winter months. For the FSF occurrence during 1800–0600 LT (Figure 2c), the maximum occurrence is in June (57%). These seasonal variations in occurrence probabilities of RSF and FSF are similar to those in the previous studies at the same location in high solar activity years of different solar cycles [*C.-M. Huang*, 1970; *Y. N. Huang et al.*, 1987].

[10] The nighttime variations in occurrence probabilities of RSF (open square line) and FSF (solid square line) are

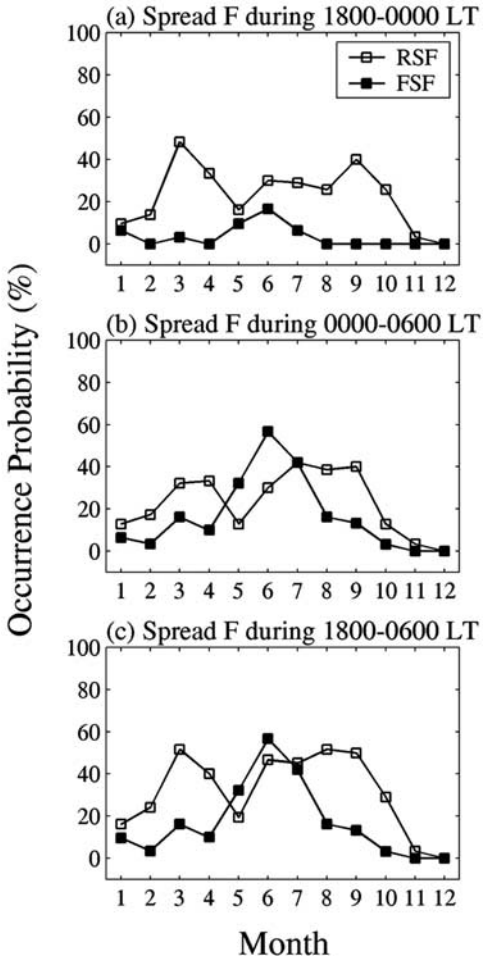

Figure 2. Seasonal variations in occurrence probabilities of RSF (open square line) and FSF (solid square line) during (a) 1800–0000, (b) 0000–0600, and (c) 1800–0600 LT. The data of spread F were observed by the Chungli ionosonde during 2000.

presented in Figure 3. It is noted that the nighttime variations are categorized into three seasons: E (March, April, September, and October), J (May, June, July, and August), and D months (January, February, November, and December). The occurrence probability is the number of spread F event in an hour divided by the number of observed ionogram in this hour for a season. In E months (Figure 3a), the RSF occurrence increases rapidly from 1900 to 2100 LT, and maintains a flat maximum (18–19%) for 3 h, then decreases gradually. For FSF, the occurrences are less than 4% during whole night. In Figure 3b, for the J months, the RSF occurrence begins to increase at 2000 LT, and peaks at 2300 LT (15%), then keeps a value of 10–13 % until 0400 LT. The FSF occurrence increases gradually from 2300 LT, and its peak value is at 0300 LT (8%). Regarding the D months (Figure 3c), both the RSF and FSF occurrences are less than 4%. These nighttime variations of occurrence probabilities shown in Figure 3 are also close to the results of *C.-M. Huang* [1970] and *Y. N. Huang et al.* [1987]. Overall, the variations in occurrence probability of RSF differ totally from those of FSF. This significant difference suggests that the generation mechanisms of RSF and FSF are not same.

[11] For the GPS phase fluctuations, two levels of Fp ($50 < Fp \leq 200$ and $200 < Fp$) detected by the S101 station are applied to the statistical study. The seasonal variations in occurrence probabilities of two Fp levels are shown in Figure 4. The occurrence probability is the percentage of days on which at least one event of phase fluctuations is recorded daily in a month. During premidnight (Figure 4a), two maximum values peak in March (32%) and September (33%) for $50 < Fp \leq 200$ (solid circle line). In Figure 4b, the $50 < Fp \leq 200$ have greater occurrences in March, April, and June–September (23–32%) during 0000–0600 LT. For whole night (1800–0600 LT), the greater occurrences of $50 < Fp \leq 200$ are generally found in the E and J months (24–43%), as shown in Figure 4c. Regarding $200 < Fp$ (open circle line), it is found in Figure 4, that the occurrence probability is very rare. This indicates that the very strong irregularities would not appear in the EIA crest region. Because the observation of GPS phase fluctuations in the EIA crest region has not been done before, we

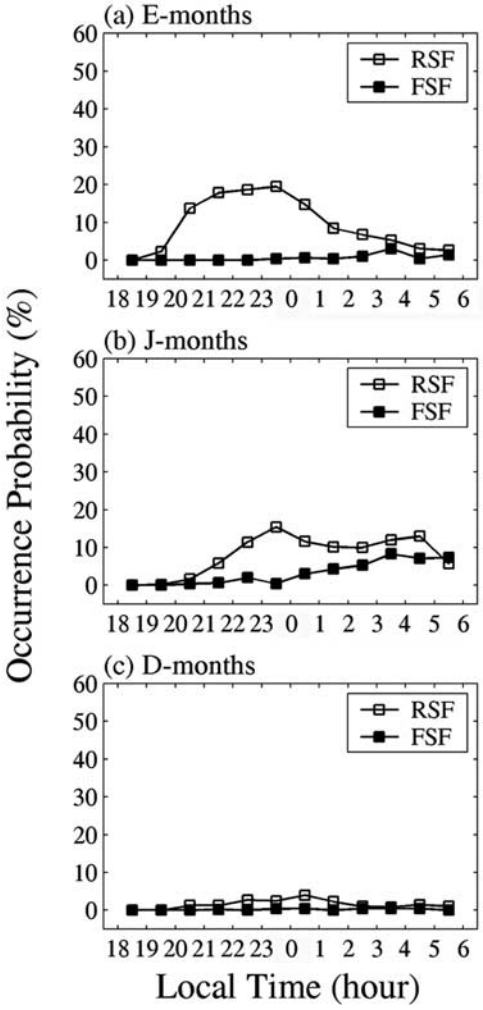

Figure 3. Nighttime variations in occurrence probabilities of RSF (open square line) and FSF (solid square line) for (a) E, (b) J, and (c) D months. The data of spread F were observed by the Chungli ionosonde during 2000.

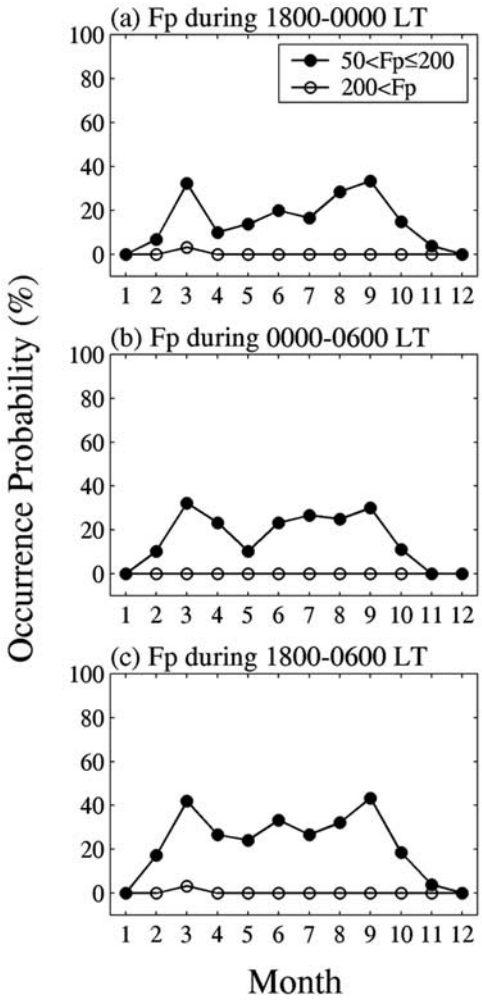

Figure 4. Seasonal variations in occurrence probabilities of $50 < Fp \leq 200$ (solid circle line) and $200 < Fp$ (open circle line) during (a) 1800–0000, (b) 0000–0600, and (c) 1800–0600 LT. The data of GPS phase fluctuations were observed by the S101 GPS receiver during 2000.

compare with the results of TEC depletion associated with amplitude scintillation at the same location [*Y. N. Huang*, 1985]. *Y. N. Huang* [1985] also found that the occurrences have two peaks in spring and autumn for premidnight, and have greater values in spring, summer, and autumn for postmidnight.

[12] Figure 5 shows that the nighttime variations in occurrence probabilities for $50 < Fp \leq 200$ (solid circle line) and $200 < Fp$ (open circle line). The occurrence probability is the number of event of phase fluctuations in an hour divided by the total number of the record in this hour in a season. Figure 5a displays that in the E months, the $50 < Fp \leq 200$ occurrence increases from 2000 to 2200 LT, and maintains a flat maximum (11–14%) for 4 h, then decreases gradually. For the J months (Figure 5b), the occurrence of $50 < Fp \leq 200$ increases gradually from 1900 LT, and reaches its maximum at 0000 LT (14%), then decreases rapidly. In Figure 5c, the event of $50 < Fp \leq 200$ is almost absent in the D months. The nighttime occurrence variations in TEC depletion associated with amplitude scintillation of *Y. N. Huang* [1985] are similar to that of $50 < Fp \leq 200$ in the current study, if some depression in the occurrence around midnight during high sunspot year (in their Figure 13) are ignored. Furthermore, this similarity would be not surprising, because the GPS phase fluctuations and TEC depletions appear simultaneously usually [e.g., *Basu et al.*, 1999; *Mendillo et al.*, 2000].

[13] For plasma bubbles at 600 km obtained from the ROSCAT-1, the seasonal variations in occurrence probabilities for premidnight (1800–0000 LT), postmidnight (0000–0600 LT), and whole night (1800–0600 LT) are presented in Figures 6a, 6b, and, 6c, respectively. The occurrence probability is the number of day on which at least one bubble event is observed in the circle (shown in Figure 1) divided by the number of day on which the ROCSAT-1 flies pass the same area in a month. It is noted that the data gaps in Figures 6a and 6b are because the number of day on which the ROCSAT-1 flies pass the circle is less than 10 days in a month. Because the number of observed day for bubble event is rare for each month, it is

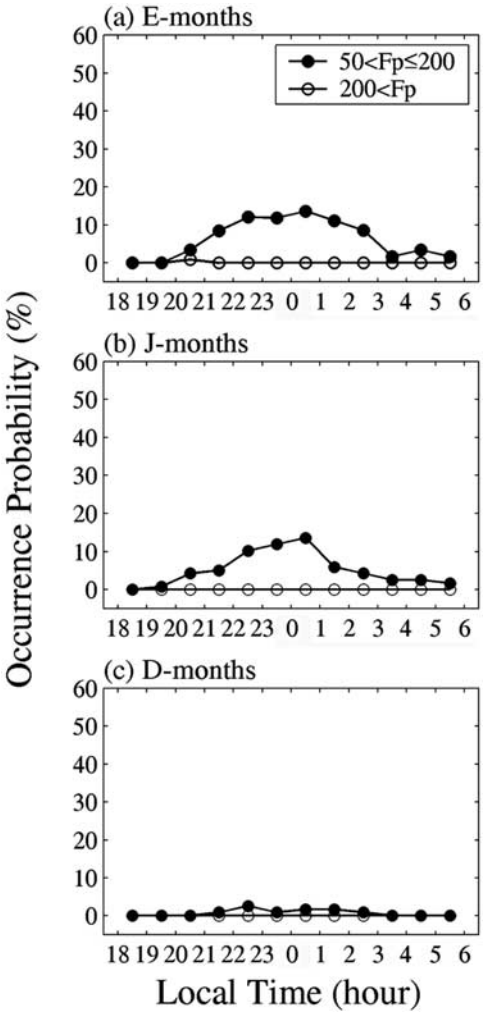

Figure 5. Nighttime variations in occurrence probabilities of $50 < Fp \leq 200$ (solid circle line) and $200 < Fp$ (open circle line) for (a) E, (b) J, and (c) D months. The data of GPS phase fluctuations were observed by the S101 GPS receiver during 2000.

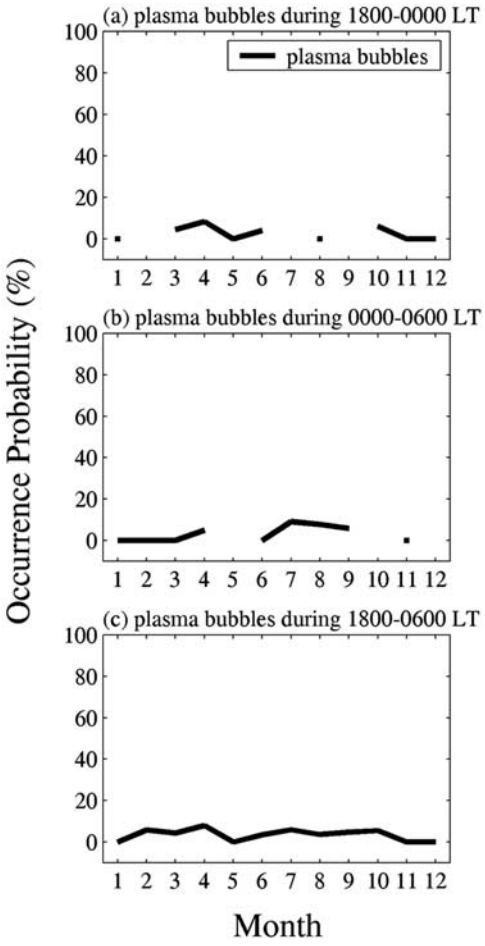

Figure 6. Seasonal variations in occurrence probability of plasma bubbles above Chungli during (a) 1800–0000, (b) 0000–0600, and (c) 1800–0600 LT. The data of plasma bubbles were observed by the ROCSAT-1 at 600 km altitude during 2000. The data gaps are due to the fact that the number of days on which the ROCSAT-1 flies past the circular area is less than 10 days in a month.

difficult to find the seasonal variation in Figure 6. Further, the rare event cannot be used to produce the nighttime variations in occurrence probability of plasma bubbles. The rare bubble phenomenon indicates that the *F* region irregularities in the EIA crest region in the western Pacific sector would occur seldom above 600 km altitude.

3.2. Comparison Between Spread F and GPS Phase Fluctuations

[14] Figure 7 displays the seasonal variations in occurrence probabilities of RSF (open square line), FSF, (gray solid square line) and $50 < p \leq 200$ (solid circle line). Generally, the seasonal variation in occurrence probability of RSF corresponds well with that of $50 < Fp \leq 200$. For detailed comparison, the nighttime variations in occurrence probabilities of RSF and $50 < Fp \leq 200$ are plotted together in Figure 8. Because the occurrences of RSF and $50 < Fp \leq 200$ are both rare in the D months, the comparison of this season is not presented in Figure 8. In Figures 8a and 8b, there are some differences between the RSF and $50 < Fp \leq 200$ occurrences existing during 2000–2300 LT and 0100–

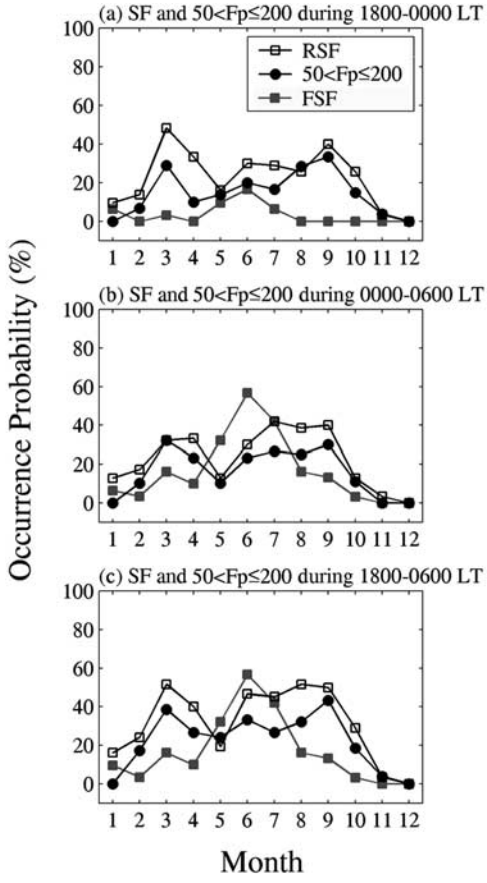

Figure 7. Seasonal variations in occurrence probabilities of $50 < Fp \leq 200$ (solid circle line), RSF (open square line), and FSF (gray solid square line) during (a) 1800–0000, (b) 0000–0600, and (c) 1800–0600 LT.

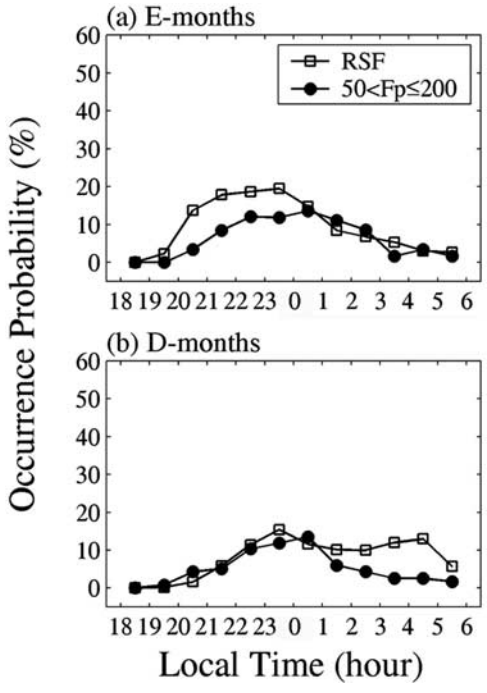

Figure 8. Nighttime variations in occurrence probabilities of $50 < Fp \leq 200$ (solid circle line) and RSF (open square line) for (a) E and (b) D months.

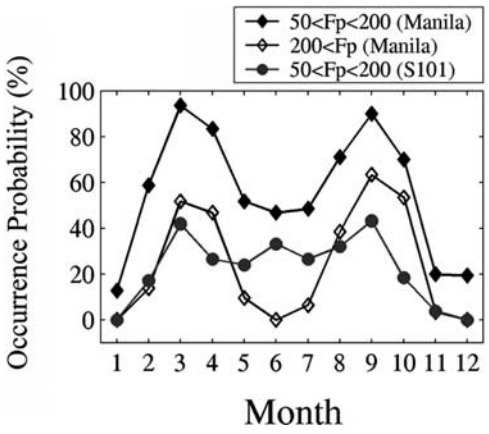

Figure 9. Seasonal variations in occurrence probabilities of $50 < Fp \leq 200$ (solid diamond line) and $200 < Fp$ (open diamond line) at Manila, as well as of $50 < Fp \leq 200$ (gray solid circle line) at S101.

0500 LT for the E and J months, respectively. These results indicate that the characteristics of *F* region irregularities forming the RSF echoes on ionogram might be not all responsible to the GPS phase fluctuations ($50 < Fp \leq 200$) in premidnight and postmidnight for the E and J months, respectively, although the $50 < Fp \leq 200$ is mainly related to RSF. On the other hand, the occurrence probability of FSF does not vary with that of $50 < Fp \leq 200$ at all. This suggests that the FSF does not induce the phase fluctuations in GPS signals.

4. Discussion

[15] In Figures 2 and 3, the seasonal and nighttime variations in occurrence probabilities of RSF are not consistent with those of FSF. This inconsistence demonstrates that the generation mechanism of RSF is obviously different from that of FSF. According to the previous studies [e.g., *Valladares et al.*, 1983; *Y. N. Huang*, 1985], RSF seems to be associated with the irregularities inside the field aligned plasma depletions which extend from the dip equator to the EIA crest; while FSF seems to be generated locally. In the following, the formation mechanisms of these two types spread F will be discussed.

[16] First, we examine the generation mechanism of RSF at the EIA crest. Since the earlier works proposed that RSF at the EIA crest is associated with the *F* region irregularities at the dip equator, we compare the occurrence probabilities of *F* region irregularities of these two locations in the western Pacific sector. For this comparison, the GPS phase fluctuations at Manila, which have been reported by *Chu et al.* [2009], are adopted. The Manila GPS data is the combined data set (by choosing the best data quality) of PIMO (14.6°N, 121.1°E, geomagnetic latitude is 6.9), TVST (14.0°N, 121.0°E, geomagnetic latitude is 6.3°N), and KAYT (14.0°N, 121.0°E, geomagnetic latitude is 6.3°N), because the above three data sets at Manila were not recorded for everyday individually (see *Chu et al.* [2009] for detail). Figure 9 displays that the seasonal variations in occurrence probabilities of $50 < Fp \leq 200$ (solid diamond line) and $200 < Fp$ (open diamond line) at Manila for 2000. It is noted that the data processes deriving the seasonal variations in occurrence probabilities at Manila is the same as those at S101. The occurrence probability of $50 < Fp \leq 200$ at Manila has the maximum, moderate, and minimum values in the E, J, and D months, respectively. This trend in the seasonal variation is also found in that at S101 (gray solid circle line in Figure 9). Therefore, the $50 < Fp \leq 200$ occurrences at the EIA crest are apparently related to those at the dip equator. Furthermore, because of the similarity in the seasonal variations of $50 < Fp \leq 200$ and RSF occurrences (Figure 7), RSF at the EIA crest can be associated with the *F* region irregularities at the dip equator. Besides, in Figure 9, it is found that the ratio of the $50 < Fp \leq 200$ occurrences in the E and J months at Manila to those at S101 is about 2:1. This ratio suggests that the possibility for that the *F* region irregularities extend from the dip equator to the EIA crest is about 50%. Nevertheless, on the basis of the similarity above, the formations of RSF and $50 < Fp \leq 200$ at the EIA crest would be mainly controlled by the generation mechanism of *F* region irregularities at the dip equator.

[17] At the dip equator, the *F* region irregularities are generated in the bottomside ionosphere usually after sunset, mainly because of the Rayleigh-Taylor (R-T) instability [e.g., *Kelley*, 1989]. On the basis of the previous studies [e.g., *Fejer et al.*, 1999; *Lee et al.*, 2005a, 2005b; *Lee*, 2006], the magnitude of the upward drift velocity of prereversal enhancement (PRE) at the dip equator play a dominant role on the variability of *F* region irregularities. This is because the PRE upward velocity can affect the growth rate of R-T instability through the gravitational and electrodynamic drift terms and by controlling the electron density gradient in the bottomside *F* region after sunset. Additionally, the late reversal time of the PRE velocity would also help the generation of *F* region irregularities in the equatorial ionosphere [e.g., *Fejer et al.*, 1999; *Lee et al.*, 2005b]. It is noted that in the west Pacific sector, the magnitude of PRE upward velocity is larger in the E months, but is smaller in the J and D months [*Fejer et al.*, 2008, Figure 7]. And, the PRE upward velocities have the latest and earliest reversal times in the J and D months, respectively [*Fejer et al.*, 2008, Figure 7].

[18] In the E months, the maximum occurrence of *F* region irregularities near the dip equator can be mainly ascribed to the larger PRE velocity, according to the previous studies [e.g., *Fejer et al.*, 1999; *Lee et al.*, 2005a, 2005b; *Lee*, 2006]. This is the reason why the $50 < Fp \leq 200$ occurrence at Manila has two peaks in March and September (Figure 9). The irregularities at the dip equator would be further lifted to higher altitudes. In order to confirm this point, the seasonal variation in occurrence probability of plasma bubbles generated from the dip equator is produced. This occurrence probability of plasma bubbles is the number of day on which at least one bubble event is observed in the rectangular area (marked by the solid lines in Figure 1) divided by the number of day on which the ROCSAT-1 flies pass the area in a month. The rectangular area is inside $0 \pm 20°$ geomagnetic latitudes and $121 \pm 5°$ geographic longitudes. The limits of $0 \pm 20°$ geomagnetic latitudes are chosen, because it is near the location of the EIA crests in both the north and south hemispheres where bubbles can be extended via the geo-

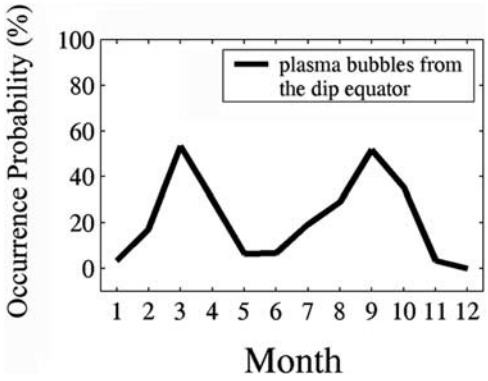

Figure 10. Seasonal variations in occurrence probabilities of plasma bubbles generated from the dip equator. The data of plasma bubbles were observed by the ROCSAT-1 at 600 km altitude during 2000.

magnetic field. On the basis of *Lee et al.* [2005a], the plasma bubbles detected in this area can be attributed the bubbles generated from the *F* region at the dip equator. In Figure 10, the two equinoctial peaks in the occurrence probability of ROCSAT-1 bubbles signify that the irregularities are lifted to altitudes higher than 600 km in this season. *Chen et al.* [2006] pointed out that the larger altitudinal distribution of irregularities would cause the larger values of *Fp*. Accordingly, these two equinoctial peaks are found in the $200 < Fp$ occurrence at Manila (Figure 9). Further, the *F* region irregularities at the dip equator, lifted to higher altitudes, will extend to higher latitudes. As a result, two equinoctial peaks are found in the RSF and $50 < Fp \leq 200$ occurrences at the EIA crest (Figures 2 and 4). Here, we draw the altitudinal/latitudinal distribution of *F* region irregularities in the E months (see the gray area in Figure 11a), on the basis of the results in section 3. In Figure 11a, the upper boundary of gray area at Chungli and S101 is placed below 600 km, because of the rare event of plasma bubbles (Figure 6). Consequently, the upper boundary at the dip equator is set below 1100 km, although the *F* region irregularities can attain to an equatorial height higher than 1500 km [e.g., *Sahai et al.*, 2000; *Su et al.*, 2006]. In Figure 11a, it is found that the altitudinal distribution of irregularities at S101 is smaller than at Manila. This difference in the altitudinal distribution might be a reason why the occurrences probability of $50 < Fp \leq 200$ at S101 is less than at Manila. Furthermore, this difference can explain that the $200 < Fp$ event appears at Manila, but not at S101.

[19] For two other seasons, the occurrences of $50 < Fp \leq 200$ at Manila in the J months are greater than those in the D months. However, the magnitudes of PRE upward velocity of these two seasons are close [*Fejer et al.*, 2008, Figure 7]. Here, the reversal time of PRE velocity is considered for the difference in occurrence between the J and D months, because the late reversal time would assist in forming the equatorial *F* region irregularities [*Fejer et al.*, 1999]. In the J months, although the magnitude of PRE velocity is smaller, the latest reversal time of PRE upward velocity would help to generating the *F* region irregularities, and in turn is responsible for the moderate occurrences of $50 < Fp \leq 200$ at Manila. On the other, in the D months, the earliest reversal time of PRE upward velocity would not support the irregularity formation. And, the magnitude of PRE upward velocity is smaller in this season. Consequently, the occurrences of $50 < Fp \leq 200$ at Manila are minimum in the D months. Furthermore, because both the occurrences of $200 < Fp$ (Figure 9) and plasma bubbles (Figure 10) are little in the J and D months, the smaller PRE velocity in these two season might be mainly responsible for the little occurrences.

[20] At the EIA crest, the occurrence probabilities of RSF and $50 < Fp \leq 200$ are moderate in the J months (Figures 2 and 4). This indicates that the smaller PRE velocity in this season can still help the equatorial *F* region irregularities extending to the EIA crest. Further, the altitudinal/latitudinal distribution of *F* region irregularities in the J months can be sketched in Figure 11b. Figure 11b illustrates that altitudinal distribution of irregularities is smaller in the J months (Figure 11b) than in the E months (Figure 11a). These altitudinal/latitudinal distributions of irregularities in Figure 11 explain why the $50 < Fp \leq 200$ occurrences are less in the J months than in the E months, both at Manila and S101. It is noted that the altitudinal distribution of irregularities at S101 is able to cause the significant phase fluctuations in GPS signals, although the distribution is smaller. Regarding the D months, because the *F* region irregularities appear seldom in the equatorial ionosphere in this season, the phenomena of RSF and $50 < Fp \leq 200$ are rare at the EIA crest, as shown in Figures 2 and 4.

[21] As the discussions above, the *F* region irregularities forming $50 < Fp \leq 200$ and RSF at the EIA crest are originated from the equatorial *F* region. However, the occurrence probabilities of RSF are slight greater than those of $50 < Fp \leq 200$ occurrences in the premidnight and postmidnight periods in the E and J months, respectively (Figures 7 and 8). The reasons for these discrepancies might be (1) the scale sizes of irregularities forming RSF and GPS phase fluctuations are different, and (2) the altitudinal distribution of irregularities is not large enough to cause GPS phase fluctuations [*Rodrigues et al.*, 2004; *Chen et al.*, 2006]. According to *Aarons et al.* [1996] and *Basu and Basu* [1993], the irregularity size for GPS phase fluctuation is few kilometers for high elevation angle and tens kilometers for low elevation angle; while spread F observed on ionogram is caused by irregularities of kilometer-scale size. Since the scale sizes of for RSF and GPS phase fluctuations are close, the irregularity sizes would not account for these discrepancies. On the other hand, these discrepancies might be ascribed to the smaller altitudinal distribution of irregularities, which is not capable of fluctuating GPS signals, but can be detected by an ionosonde.

[22] Next, we discuss the formation mechanism of FSF at the EIA crest. Since the seasonal variation in occurrence probability of FSF differs from that of RSF, the formation of FSF would be not related to the equatorial *F* region irregularities. *Y. N. Huang* [1985] suggested that FSF seems to be generated locally. In this work, we find that the occurrence probability of FSF of the current study is similar to that of spread F at midlatitudes in the western Pacific sector [*Shiokawa et al.*, 2003]. In Figure 12, the occurrence probabilities of spread F observed by five ionosondes in Japan, adopted from *Shiokawa et al.* [2003], have a peak in June or July during high solar activity. The June peak also appears in the FSF occurrence of the current study (solid

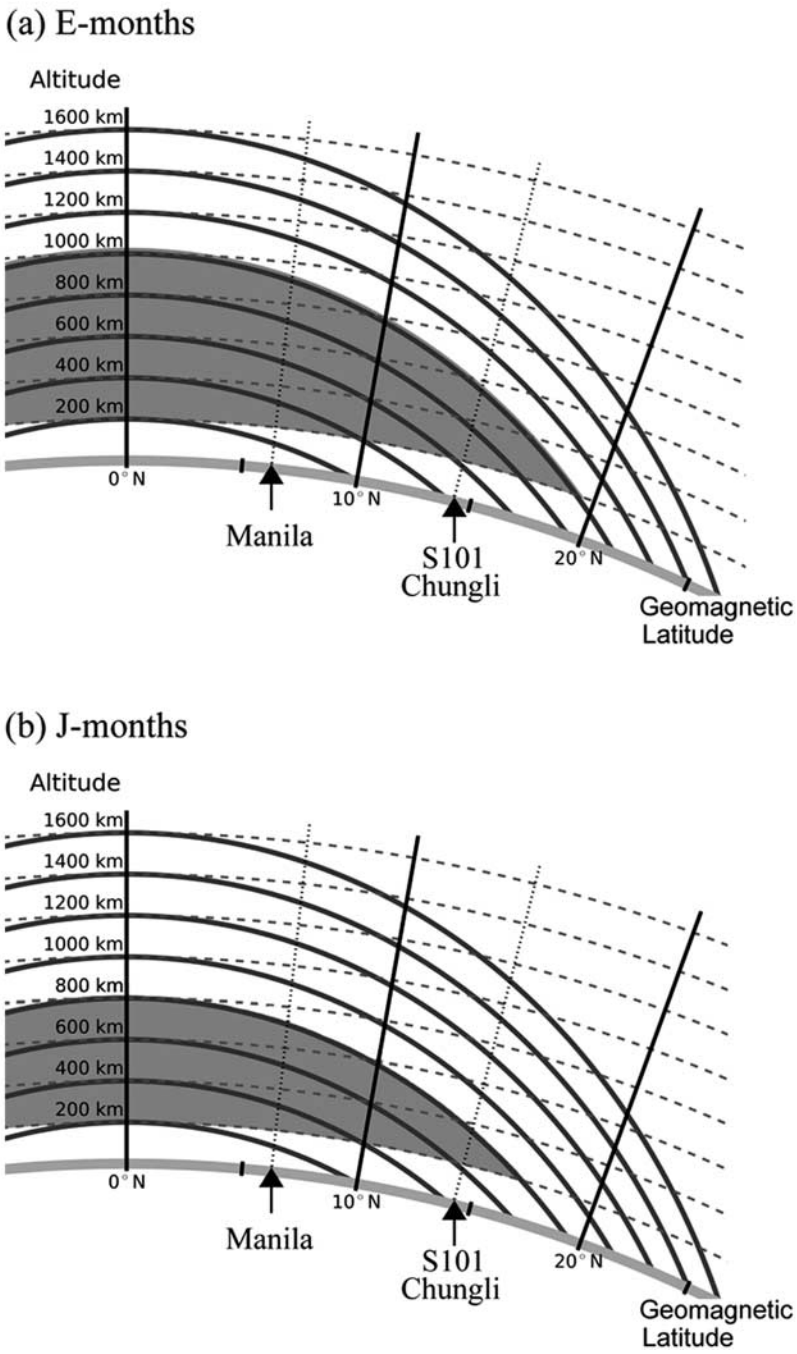

Figure 11. The sketches of altitudinal/latitudinal distribution of *F* region irregularities for the (a) E and (b) J months. The gray areas represent the distribution of irregularities.

square line). This result indicates that the formation mechanisms for FSF at the EIA crest and spread F at midlatitudes could be similar.

[23] For spread F at midlatitudes, the Perkins instability [*Perkins*, 1973] was used to interpret the observations of *F* region irregularities [e.g., *Fukao et al.*, 1991; *Kelley and Fukao*, 1991]. However, the growth rate of the Perkins instability might be too low to generate any significant irregularity in *F* region [e.g., *Kelley and Fukao*, 1991]. Additionally, the medium-scale traveling ionospheric disturbances (MSTIDs) might generate the midlatitude spread F [e.g., *Bowman*, 1990; *Shiokawa et al.*, 2003]. It is noted that *Shiokawa et al.* [2003] pointed out the coincidence of the spread F and the MSTIDs in only 10–15%, although they showed the occurrence probability of MSTIDs also has a summer peak. Recently, some studies applied the coupled *E*/*F* region electrodynamics to explain observational properties of midlatitude spread F [*Cosgrove and Tsunoda*, 2003; *Haldoupis et al.*, 2003]. This mechanism is able to generate the *F* region irregularities more rapidly than by the Perkins instability acting alone. Although some observation results of midlatitude spread F can be interpreted by these mechanisms, the mechanism generating the midlatitude spread F is not specified yet. Accordingly, the further study

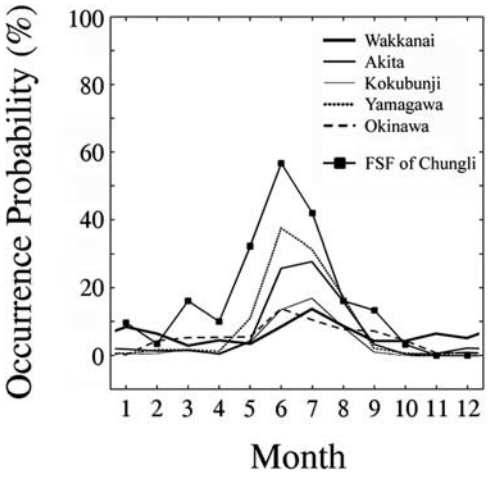

Figure 12. Occurrence probabilities of spread F at midlatitudes and FSF at Chungli. The occurrence probabilities of spread F at midlatitudes, observed by five ionosondes in Japan, are adopted from *Shiokawa et al.* [2003].

is necessary to investigate the FSF mechanisms, even if the formation mechanisms for FSF at the EIA crest are the same as those for spread F at midlatitudes.

5. Conclusion and Summary

[24] In this study, we conduct the Chungli ionosonde, S101 GPS receiver, and ROCSAT-1 to investigate the *F* region irregularities at the EIA crest. The occurrence probabilities of spread F, GPS phase fluctuations, and plasma bubbles are concurrently analyzed for the first time. The period of data used in this study is during 2000, which is the solar maximum year in the 23rd solar cycle. The analysis leads to the following conclusions.

[25] The seasonal variation in occurrence probability of RSF has the maximum, moderate, and minimum values in the E, J, and D months. For the nighttime variation, RSF occurrence peaks at 2300 LT. Regarding the FSF occurrence, the maximum values in the seasonal variation is in June, and the nighttime variation has a peak at 0300 LT. These results demonstrate that the seasonal and nighttime variations in occurrence probability of RSF are different from those of FSF. Further, these suggest that the formation mechanism of RSF is not the same as that of FSF. For the GPS phase fluctuations, the seasonal variation in occurrence probability of $50 < Fp \leq 20$ is maximum, moderate, and minimum in the E, J, and D months. The variations in occurrence probability of $50 < Fp \leq 200$ are similar to those of RSF. This similarity demonstrates that the characteristics of *F* region irregularities causing $50 < Fp \leq 200$ are mainly controlled by those forming RSF. Nevertheless, the slight discrepancies existing between the RSF and $50 < Fp \leq 200$ occurrences indicate that the *F* region irregularities forming RSF are not all responsible to the GPS phase fluctuations ($50 < Fp \leq 200$). In addition, the very rare occurrence of $200 < Fp$ suggests that the *F* region irregularities cannot cause the strong level of phase fluctuations in GPS signal. Regarding the plasma bubbles, the infrequent event observed by ROCSAT-1 implies that the irregularities occur seldom above 600 km at the EIA crest.

[26] The comparison of GPS phase fluctuations between at S101 and at Manila shows that the trends of seasonal variations in $50 < Fp \leq 200$ occurrence of these two locations are similar. Therefore, the *F* region irregularities for RSF and $50 < Fp \leq 200$ at the EIA crest are extended from the equatorial ionosphere along the geomagnetic field lines. Since the magnitude and the reversal time of the PRE upward velocity at the dip equator can affect the occurrence probability of the equatorial *F* region irregularities, these two characteristics of the PRE velocity would be also mainly associated to the occurrence probabilities of RSF and $50 < Fp \leq 200$ at the EIA crest. In the E and D months, the maximum and minimum occurrences of RSF and $50 < Fp \leq 200$ at the EIA crest are associated with the larger and smaller PRE velocities at the dip equator, respectively. Because the magnitude of PRE velocity is smaller but the reversal time of PRE velocity is the latest in the J months, the occurrences of RSF and $50 < Fp \leq 200$ at the EIA crest are moderate.

[27] The seasonal variation in occurrence probability of FSF at the EIA crest is found to be similar to that in the midlatitude spread F. The June peak exists in the occurrence probabilities of both FSF at the EIA crest and spread F at midlatitude. The generation mechanisms of the midlatitude spread F might be applied to explain the formation of FSF at the EIA crest. However, the further study is needed to find whether the mechanisms are suitable for FSF.

[28] **Acknowledgments.** This work is supported by the grants of National Space Organization 98-NSPO(B)-IC- FA07–01(R) and National Science Council NSC 98-2119-M-231-001. W.S.C. is supported by NSC 97-2811-M-008-042. S.-Y.S. is supported by NSC 97-2811-M-008-013. We also thank Institute of Earth Sciences, Academia Sinica, Taipei, Taiwan, for providing GPS data.

[29] Zuyin Pu thanks Harish Chandra and Yuichi Otsuka the reviewers for their assistance in evaluating this paper.

References

Aarons, J., M. Mendillo, R. Yantosca, and E. Kudeki (1996), GPS phase fluctuations in the equatorial region during the MISETA 1994 campaign, *J. Geophys. Res.*, *101*, 26,851–26,862, doi:10.1029/96JA00981.

Anderson, D. N. (1973a), A theoretical study of the ionospheric *F* region equatorial anomaly—Part I. Theory, *Planet. Space Sci.*, *21*, 409–419, doi:10.1016/0032-0633(73)90040-8.

Anderson, D. N. (1973b), A theoretical study of the ionospheric *F* region equatorial anomaly—Part II. Results in the American and Asian sectors, *Planet. Space Sci.*, *21*, 421–442, doi:10.1016/0032-0633(73)90041-X.

Appleton, E. V. (1946), Two anomalies in the ionosphere, *Nature*, *157*, 691, doi:10.1038/157691a0.

Basu, S., and S. Basu (1993), Ionospheric structure and scintillation spectra, in *Wave Propagation in Random Media (Scintillation)*, edited by V. I. Tatarskii, A. Ishimaru, and V. U. Zavorotny, pp. 139–155, Soc. for Opt. Eng., Bellingham, Wash.

Basu, S., K. M. Groves, J. M. Quinn, and P. Doherty (1999), A comparison of TEC fluctuations and scintillations at Ascension Island, *J. Atmos. Sol. Terr. Phys.*, *61*, 1219–1226, doi:10.1016/S1364-6826(99)00052-8.

Bowman, G. G. (1990), A review of some recent work on mid-latitude spread-F occurrence as detected by ionosondes, *J. Geomag. Geoelectr.*, *42*, 109–138.

Bramley, E. N., and M. Peart (1965), Effect of ionization transport on the equatorial *F* region, *Nature*, *206*, 1245–1246, doi:10.1038/2061245a0.

Chakraborty, S. K., A. DasGupta, S. Ray, and S. Banerjee (1999), Long-term observation of VHF scintillation and total electron content near the crest of the equatorial anomaly in the Indian longitude zone, *Radio Sci.*, *34*, 241–255, doi:10.1029/98RS02576.

Chandra, H., S. Sharma, M. A. Abdu, and I. S. Batista (2003), Spread-F at anomaly crest regions in the Indian and American longitudes, *Adv. Space Res.*, *31*, 717–727, doi:10.1016/S0273-1177(03)00034-6.

Chen, W. S., C. C. Lee, J. Y. Liu, F. D. Chu, and B. W. Reinisch (2006), Digisonde spread F and GPS phase fluctuations observed in the equatorial ionosphere during solar maximum, *J. Geophys. Res.*, *111*, A12305, doi:10.1029/2006JA011688.

Chu, F. D., C. C. Lee, W. S. Chen, and J. Y. Liu (2008), A study of long-term climatology of ionospheric irregularities by using GPS phase fluctuations at the Brazilian longitudes, *Adv. Space Res.*, *41*, 645–649, doi:10.1016/j.asr.2007.05.003.

Chu, F. D., W. S. Chen, C. C. Lee, and J. Y. Liu (2009), A climatological study of nocturnal equatorial *F* region irregularities at the west Pacific longitudes by using phase fluctuations of the global positioning system, *J. Atmos. Sol. Terr. Phys.*, in press.

Cosgrove, R. B., and R. T. Tsunoda (2003), Simulation of the nonlinear evolution of the sporadic E layer instability in the nighttime midlatitude ionosphere, *J. Geophys. Res.*, *108*(A7), 1283, doi:10.1029/2002JA009728.

DasGupta, A., A. Maritra, and S. Basu (1981), Occurrence of nighttime VHF scintillations near the equatorial anomaly crest in the Indian sector, *Radio Sci.*, *16*, 1455–1458, doi:10.1029/RS016i006p01455.

Davies, K. (1990), *Ionospheric Radio*, Peter Peregrinus Ltd., London.

Fejer, B. G., L. Scherliess, and E. R. de Paula (1999), Effects of the vertical plasma drift velocity on the generation and evolution of equatorial spread F, *J. Geophys. Res.*, *104*, 19,859–19,869, doi:10.1029/1999JA900271.

Fejer, B. G., J. W. Jensen, and S.-Y. Su (2008), Quiet time equatorial *F* region vertical plasma drift model derived from ROCSAT-1 observations, *J. Geophys. Res.*, *113*, A05304, doi:10.1029/2007JA012801.

Fukao, S., M. C. Kelley, T. Shirakawa, T. Takami, M. Yamameto, T. Tsuda, and S. Kato (1991), Turbulent upwelling of the midlatitude ionosphere: 1. Observational results by the MU radar, *J. Geophys. Res.*, *96*, 3725–3746, doi:10.1029/90JA02253.

Haldoupis, C., M. C. Kelley, G. C. Hussey, and S. Shalimov (2003), Role of unstable sporadic E layers in the generation of midlatitude spread F, *J. Geophys. Res.*, *108*(A12), 1446, doi:10.1029/2003JA009956.

Huang, C.-M. (1970), *F* region irregularities that cause scintillations and spread-F echoes at low-latitude, *J. Geophys. Res.*, *75*, 4833–4841, doi:10.1029/JA075i025p04833.

Huang, Y. N. (1985), Ionospheric electron content depletion associated with amplitude scintillation at the equatorial anomaly crest zone, *J. Geophys. Res.*, *90*, 4333–4339, doi:10.1029/JA090iA05p04333.

Huang, Y. N., K. Cheng, and W. T. Huang (1987), Seasonal and solar cycle variations of spread F at the equatorial anomaly crest zone, *J. Geomag. Geoelectr.*, *39*, 639–657.

Kelley, M. C. (1989), *The Earth's Ionosphere*, *Int. Geophys. Ser*, vol. 43, Academic, San Diego, Calif.

Kelley, M. C., and S. Fukao (1991), Turbulent upwelling of the midlatitude ionosphere: 2. Theoretical framework, *J. Geophys. Res.*, *96*, 3747–3753, doi:10.1029/90JA02252.

Kulkarni, P. P., and R. G. Rastogi (1969), Spread-F echoes at Ahmedabad over a solar cycle, *Ann. Geophys.*, *25*, 577–587.

Lee, C. C. (2006), Examine the local linear growth rate of collisional Rayleigh-Taylor instability during solar maximum, *J. Geophys. Res.*, *111*, A11313, doi:10.1029/2006JA011925.

Lee, C. C., S.-Y. Su, and B. W. Reinisch (2005a), Concurrent study of bottomside spread F and plasma bubble events in the equatorial ionosphere during solar maximum using Digisonde, and ROCSAT-1, *Ann. Geophys.*, *23*, 3473–3480.

Lee, C. C., J. Y. Liu, B. W. Reinisch, W. S. Chen, and F. D. Chu (2005b), The effects of the pre-reversal $\mathbf{E} \times \mathbf{B}$ drift, the EIA asymmetry, and magnetic activity on the equatorial spread F during solar maximum, *Ann. Geophys.*, *23*, 745–751.

Mendillo, M., B. Lin, and J. Aarons (2000), The application of GPS observations to equatorial aeronomy, *Radio Sci.*, *35*, 885–904, doi:10.1029/1999RS002208.

Moffett, R. J., and W. B. Hanson (1965), Effect of ionization transport on the equatorial *F* region, *Nature*, *206*, 705–706, doi:10.1038/206705a0.

Mullen, J. P., E. MacKenzie, S. Basu, and H. Whitney (1985), UHF/GHz scintillation observed at Ascension island from 1980 through 1982, *Radio Sci.*, *20*, 357–365, doi:10.1029/RS020i003p00357.

Perkins, F. (1973), Spread F and ionospheric currents, *J. Geophys. Res.*, *78*, 218–226, doi:10.1029/JA078i001p00218.

Rodrigues, F. S., E. R. de Paula, M. A. Abdu, A. C. Jardim, K. N. Iyer, P. M. Kintner, and D. L. Hysell (2004), Equatorial spread F irregularity characteristics over São Luís, Brazil, using VHF radar and GPS scintillation techniques, *Radio Sci.*, *39*, RS1S31, doi:10.1029/2002RS002826.

Sahai, Y., P. R. Fagundes, and J. A. Bittencourt (2000), Transequatorial *F* region ionospheric plasma bubbles: Solar cycle effects, *J. Atmos. Sol. Terr. Phys.*, *62*, 1377–1383, doi:10.1016/S1364-6826(00)00179-6.

Shiokawa, K., C. Ihara, Y. Otsuka, and T. Ogawa (2003), Statistical study if nighttime medium-scale traveling ionospheric disturbances using midlatitude airglow images, *J. Geophys. Res.*, *108*(A1), 1052, doi:10.1029/2002JA009491.

Su, S.-Y., C. H. Liu, H. H. Ho, and C. K. Chao (2006), Distribution characteristics of topside ionospheric density irregularities: Equatorial versus midlatitude regions, *J. Geophys. Res.*, *111*, A06305, doi:10.1029/2005JA011330.

Valladares, C. E., W. B. Hanson, J. F. McClure, and B. L. Cragin (1983), Bottomside sinusoidal irregularities in the equatorial *F* region, *J. Geophys. Res.*, *88*, 8025–8042, doi:10.1029/JA088iA10p08025.

W. S. Chen, Y. A. Liou, J. Y. Liu, and S.-Y. Su, Graduate Institute of Space Science, National Central University, 300 Jhongda Road, Jhongli 32001, Taiwan.

F. D. Chu, National Standard Time and Frequency Laboratory, Telecommunication Laboratories, Chunghwa Telecom Company, Ltd., P. O. Box 71, Jhongli 320, Taiwan.

C. C. Lee, General Education Center, Ching Yun University, 229 Jiansing Road, Jhongli 320, Taiwan. (cclee@cyu.edu.tw)

S. B. Yu, Institute of Earth Sciences, Academia Sinica, 128 Academia Road, Section 2, Taipei 11529, Taiwan.